Antiferromagnetism and magnetic frustration in the metalorganic compounds MCl_2-4SC$(NH_2)_2$, M = (Mn,Fe)

H. Fabrelli [1], A. Paduan-Filho [1], M. A. Continentino [2] and R. S. Freitas [1,*]

[1] *Instituto de Física, Universidade de São Paulo, 05508-090 São Paulo, São Paulo, Brazil*

[2] *Centro Brasileiro de Pesquisas Físicas, 22290-180 Rio de Janeiro, Rio de Janeiro, Brazil*

(Received 4 February 2022; accepted 25 March 2022; published 7 April 2022)

We report magnetic and specific heat measurements at low temperatures (>100 mK) and high magnetic fields (up to 9 T) for the metalorganic compounds $MnCl_2$-4SC$(NH_2)_2$ (DTM) and $FeCl_2$-4SC$(NH_2)_2$ (DTF). Fits to the experimental data from the Curie-Weiss law and mean-field theory indicate the antiferromagnetic nature of both compounds. For temperatures down to $T = 0.56$ K the compound DTM exhibits two successive transitions, which may be associated with different magnetic orderings. In this system the external magnetic field is a tuning parameter that allows us to access such magnetic phases separated by distinct quantum critical points. No indication of magnetic ordering is found in DTF down to 100 mK, making this compound a candidate for a strongly frustrated material with frustration parameter $f = |\theta_{CW}|/T_N > 100$. Finally, we discuss the absence of Bose-Einstein condensation of magnons and the possibility of a spin-orbital liquid state in DTF.

DOI: 10.1103/PhysRevB.105.134405

I. INTRODUCTION

In the past few decades, we have witnessed growing interest in the phenomenon of Bose-Einstein condensation (BEC) as well as its realization in different physical systems such as diluted gases [1,2], exciton-polaritons in semiconductor cavities [3], and ferromagnetic [4] and field-induced antiferromagnetic materials [5].

Especially in the case of quantum magnets, the search for materials in which the BEC of magnons occurs is currently a fertile research field leading to the discovery of dozens of examples. One of the most remarkable examples is the well-known metalorganic compound $NiCl_2$-4SC$(NH_2)_2$ (DTN), in which the quantum critical points (QCPs) associated with the BEC quantum phase transition occur for sufficiently low fields ($\mu_0 H_{c1} = 2.2$ T and $\mu_0 H_{c2} = 12.6$ T) [6–8] in comparison with other materials [5].

DTN is an $S = 1$ system which, according to the Haldane conjecture for integer spin systems, presents a large-D energy gap that separates a nonmagnetic ground state from the lowest-lying exited state. With the application of external magnetic fields, the gap closes in the QCP that separates a nonmagnetic phase from the field-induced antiferromagnetic phase that belongs to the BEC universality class with dynamical exponent $z = 2$.

Besides the realization of BEC of magnons, quantum magnets provide a pathway for the observation of other QCPs by closing the energy gap from ion substitution, as in the case of the Br-doped DTN, in which the disorder promotes the appearance of Bose-Glass and Mott-Glass phases [9], or by applying an external pressure, as in the case of the compounds $TlCuCl_3$ [10–14], $(CH_3)_2CHNH_3CuCl_3$ (IPA-$CuCl_3$) [15], $(C_4H_{12}N_2)Cu_2Cl_6$ (PHCC) [16], and $CsFeCl_3$ [17], in which such pressure-induced QCPs belong to a different universality class from the field-induced BEC QCP, presenting a linear single-particle dispersion ($z = 1$) [5].

Other studies in some of these systems focus on the effects of magnetic frustration, where the frustrated interactions between layers may lead to a dimensional reduction of the BEC QCP, as discussed for the compound $BaCuSi_2O_6$ [18]. Also, the impossibility of simultaneously satisfying competing interactions in a frustrated magnet leads to a highly degenerate ground state. As a consequence, instead of condensing in a single-particle state, bosons in a frustrated system can condense in more than one single-particle state.

An interesting direction in the research field of quantum magnets is to explore what kinds of physical phenomena and similarities, if they exist, would display compounds similar to those known examples. In the case of DTN, these compounds are made from the complete substitution of the Ni^{2+} magnetic ions for different magnetic ions, such as Mn^{2+} and Fe^{2+}.

Although many works have been devoted to studying the compound DTN, very few have explored the physics behind its manganese and iron analogs, $MnCl_2$-4SC$(NH_2)_2$ (DTM) and $FeCl_2$-4SC$(NH_2)_2$ (DTF). For DTM some AC magnetic susceptibility measurements at $\mu_0 H = 0$ T pointed to the existence of an antiferromagnetic transition at $T = 0.56$ K [19]. Later, specific heat measurements did not show indications of phase transitions [20]. In the case of DTF no indication of magnetic ordering was identified for magnetic measurements down to 4 K [21].

In the present work we study both DTM and DTF through magnetization, magnetic susceptibility, and specific heat measurements at temperatures down to 100 mK and magnetic fields up to 9 T. Our experimental results are compared to the mean-field theory expressions in order to estimate the magnitude and modulus of exchange interactions,

*freitas@if.usp.br

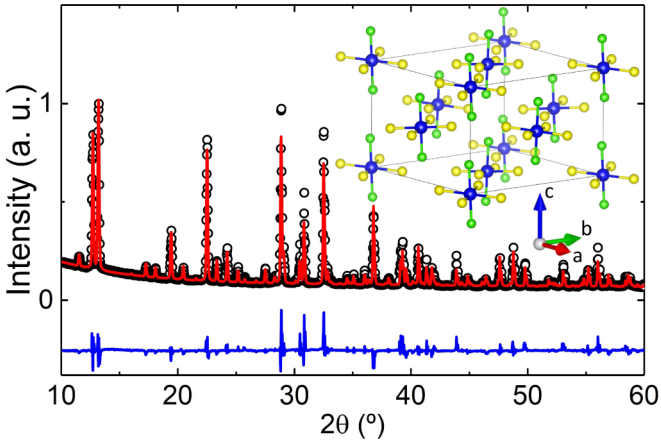

FIG. 1. Diffraction pattern of DTM. Black circles are from the measurement, the red line is the fit from the Rietveld analysis, and the blue line represents the difference between the experimental data and the fitting. Inset: Simplified structure of DTM, where blue, green, and yellow spheres are Mn, Cl, and S atoms, respectively. C, N, and H atoms were omitted for clarity.

single-ion anisotropy term D, and the g factor for both compounds.

This paper is divided as follows. In Sec. II we describe the synthesis of the MCl_2-4SC$(NH_2)_2$ (M = Mn,Fe) compounds and the experimental techniques to characterize them. The results for magnetic susceptibility, magnetization, and specific heat as well as a theoretical analysis of the results are presented in Sec. III. We conclude our discussions and present perspectives for further studies in Sec. IV. The derivation of mean-field expressions used to fit the experimental results is given in the Appendix.

II. EXPERIMENTAL DETAILS

The samples studied in this work were obtained from the method of slow evaporation of supersaturated solutions. In the case of DTN, DTM, and their nonmagnetic analog compound $CdCl_2$-4SC$(NH_2)_2$ (DTC) the solutes were dissolved in water, filtered after total dissolution, and kept in a thermal bath at a constant temperature of 38 °C. Dark yellow rectangular-prism-shaped DTN samples (the $I4$ space group) with a typical size of $3 \times 3 \times 10$ mm^3 grow in a week. The face-centered tetragonal structures of DTM [20] and DTC (the $P4_2/n$ space group; see the inset in Fig. 1) crystallized into white bipyramidal samples with sizes up to $8 \times 8 \times 8$ mm^3 that were obtained within a month.

DTF also belongs to the $P4_2/n$ space group, and samples were also grown using the method of supersaturated solution [22]. However, in this case we used ethanol as the solvent. After the complete dissolution of the solutes, the solutions were kept at 0 °C. In a matter of 2 days, dark green bipyramidal-shaped crystals with a maximum size of $3 \times 3 \times 2$ mm^3 formed. The green color of the samples is due to the imprisonment of O_2 molecules in the crystal lattice [23]. After the application of heat (80 °C for 1 h, in our case) the crystals completely release the O_2 molecules, turning a pale-yellow color.

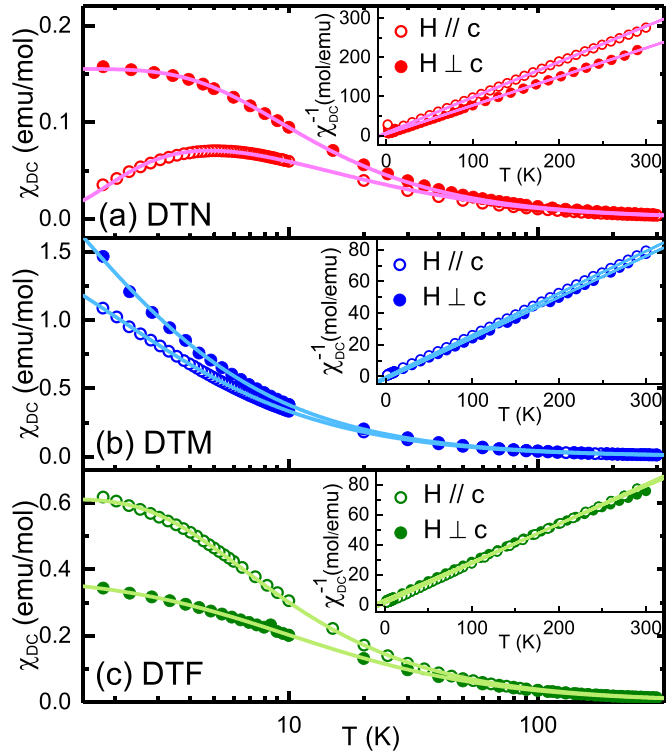

FIG. 2. $\chi_{DC}(T)$ measurements in different crystal orientations, with the external magnetic field $\mu_0 H = 0.01$ T applied parallel (//) and perpendicular (⊥) to the c axis in the range of temperatures from 1.8 to 300 K for (a) DTN, (b) DTM, and (c) DTF. Solid lines are fits from Eq. (1). Insets: Inverse of $\chi_{DC}(T)$ for each aforementioned compound with linear fits (solid lines) from the Curie-Weiss law.

For all samples we performed powder x-ray diffraction analysis and confirmed that the samples were the ones expected. In Fig. 1 we present the diffraction pattern of DTM, from which we obtained $a = b = 13.760(1)$ Å and $c = 9.065(2)$ Å. The goodness of fit obtained is $S = 6.59$.

Magnetization and magnetic susceptibility measurements in temperatures down to 1.8 K and applied magnetic field up to 7 T were performed in a magnetic property measuring system superconducting quantum interference device magnetometer from Quantum Design and in a home-built magnetometer at temperatures down to 0.5 K by pumping ^{3}He. Magnetic susceptibility measurements down to 200 mK at zero applied magnetic field were performed in a cryostat with an adiabatic demagnetization refrigerator. Specific heat measurements were taken in a physical property measurement system 9 T platform from Quantum Design with a dilution refrigerator option for temperatures down to 50 mK.

III. RESULTS

A first glimpse of the magnetic properties of DTM and DTF is given by temperature-dependent magnetization measurements. In Fig. 2 we present $\chi_{DC}(T) = M(T)/H$ measurements for DTN, DTM, and DTF for temperatures down to 1.8 K and external magnetic field $\mu_0 H = 0.01$ T applied parallel and perpendicular to the c axis.

Regarding the perpendicular orientation ($H \perp c$) of the samples, we performed $\chi_{DC}(T)$ measurements for $H \perp c$ and

TABLE I. Values of θ_{CW}, J/k_B, D/k_B (in K), and g obtained from the Curie-Weiss (CW) law and the mean-field theory fittings of $\chi_{DC}(T)$ curves in Fig. 2.

	DTN		DTM		DTF	
	$H \parallel c$	$H \perp c$	$H \parallel c$	$H \perp c$	$H \parallel c$	$H \perp c$
θ_{CW}	−6.52	−6.28	−1.52	−1.06	−1.89	−10.15
p_{CW}	2.95	3.31	5.59	5.84	5.42	5.51
$p_{\chi DC}$	3.07	3.23	5.59	5.83	5.61	5.49
g_{CW}	2.08	2.34	1.89	1.97	2.21	2.25
$g_{\chi DC}$	2.17	2.29	1.89	1.97	2.29	2.24
D/k_B	7.62	7.53	−0.17	0.15	1.42	1.44
zJ/k_B	4.93	3.53	0.73	0.44	0.37	4.76

also for another perpendicular orientation with a rotation of (+90°) from the previous one. However, no appreciable difference is observed between measurements with $H \perp c$ and $H \perp c$ (+90°) in both DTM and DTF, which suggest they possess uniaxial magnetic anisotropy.

The results in Fig. 2 show no indication of a magnetic transition for such values of temperatures and external magnetic field. We compare our experimental results in Fig. 2 with a mean-field expression for the magnetic susceptibility given by [24]

$$\chi(T) = \frac{\chi_0(T)}{1 + K\chi_0(T)}, \tag{1}$$

with $K = 2zJ/Ng^2\mu_B^2$, where z is the coordination number, J is the exchange constant, N is the number of magnetic ions, g is the gyromagnetic factor, μ_B is the Bohr magneton, and $\chi_0(T)$ is the zero-field magnetic susceptibility calculated for a single ion. In the Appendix we present the zero-field magnetic susceptibility expressions calculated for single ions with $S = 1$, $S = 2$, and $S = 5/2$, corresponding to the electron spins of the Ni^{2+}, Fe^{2+}, and Mn^{2+} ions, respectively.

The fitted curves in Fig. 2 display very good agreement with the experimental results, from which we estimate values of J/k_B, D/k_B, and g. Additionally, we compare the inverse of $\chi_{DC}(T)$ (insets in Fig. 2) with the Curie-Weiss law $\chi(T) = C(T - \theta_{CW})^{-1}$, where $C = Ng^2\mu_B^2/3k_B$, obtaining values of θ_{CW}. We summarize these results in Table I. The obtained values for p and g are in good agreement with the representative values from the literature [25]. In the case of DTN and DTM, the fitting from the Curie-Weiss law gives values of θ_{CW} of the same order of magnitude in both parallel and perpendicular orientations. For DTF, the value of θ_{CW} estimated for the perpendicular orientation is an order of magnitude higher than the value for the parallel orientation. Also this value is about 1.5 times greater than for DTN, which suggests a manifestation of the antiferromagnetic ordering for temperatures comparable to those for the DTN ($T_N^{max} = 1.2$ K) [6–8], which is reinforced by the estimation of zJ/k_B for DTN and DTF.

We also performed magnetization measurements as a function of H for DTM and DTF at different temperatures. The experimental data are also compared to the single-ion expressions for $M(H)$ from the Appendix. These results are presented in Fig. 3.

We observe a good fit with the experimental data for both compounds for the curves measured with H applied along the parallel and perpendicular directions and temperatures down to 2 K. Particularly, in the case of DTF the agreement between the experimental data and the single- ion $M(H)$ expressions presents significant deviations at lower temperatures. This deviation from the paramagnetic behavior may indicate a tendency of magnetic ordering for DTF below 2 K.

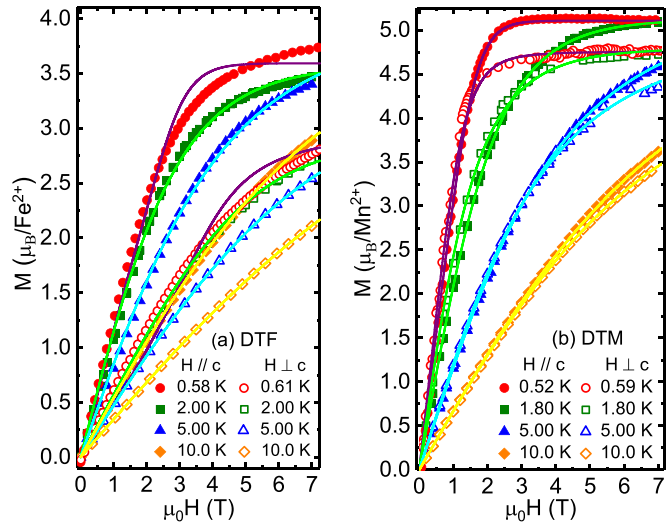

FIG. 3. Magnetization per ion as a function of $\mu_0 H$ for (a) DTF and (b) DTM measured at different temperatures. Solid lines are fitting obtained for the single-ion expressions presented in Appendix.

Measurements of $\chi_{DC}(T)$ at $\mu_0 H = 0.1$ T for DTM in different orientations as well as $\chi_{AC}(T)$ measurements of the DTF powder sample at $\mu_0 H = 0$ T, $h_{AC} = 10$ Oe, and $f = 155$ Hz are presented in Fig. 4 and compared to mean-field theory from Eq. (1). The DTM $\chi_{DC}(T)$ curves present a kink below 0.6 K, which is an indication of phase transition. According to Fisher [26], the transition temperature corresponds approximately to the inflection point of $\chi(T)$ curves, indicated by arrows in Fig. 4(a). The mean-field fitting provides good agreement with the experimental data for

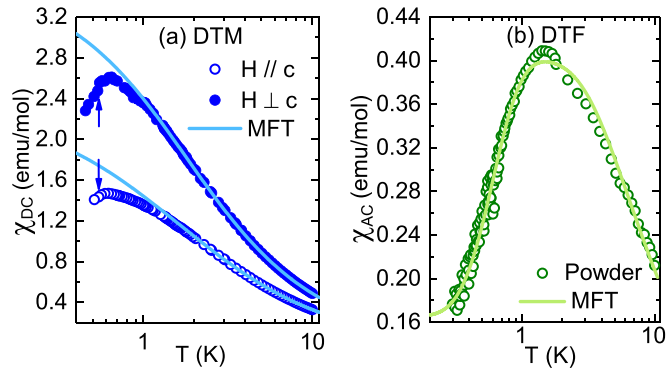

FIG. 4. (a) $\chi_{DC}(T)$ curves for DTM measured under an external magnetic field $\mu_0 H = 0.1$ T with the magnetic field applied parallel and perpendicular to the c axis. The arrows indicate the position of the inflection point of such curves. (b) $\chi_{AC}(T)$ curve at $\mu_0 H = 0$ T and $h_{AC} = 10$ Oe and $f = 155$ Hz for the DTF powder sample. Solid lines are fits obtained from the mean-field theory (MFT) from Eq. (1).

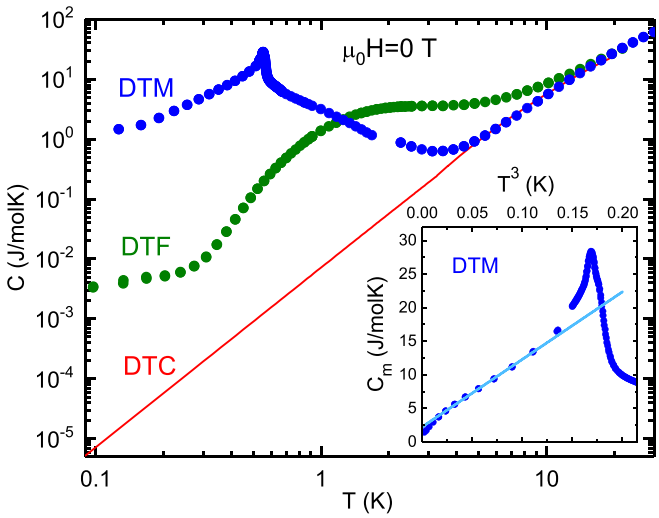

FIG. 5. Specific heat of DTM, DTF, and DTC at $\mu_0 H = 0$ T. Inset: Magnetic contribution to the specific heat of DTM as a function of T^3 and a linear fit at low temperatures (see text).

temperatures above the transition. Regarding DTF, the $\chi_{AC}(T)$ measurements [Fig. 4(b)] display a broad maximum around $T = 1.5$ K which is well fitted by the mean-field theory.

Along with magnetization and magnetic susceptibility measurements we also performed specific heat measurements for the DTM and DTF samples as well as for the nonmagnetic analog compound DTC. These results, at $\mu_0 H = 0$ T, are presented in Fig. 5.

The existence of a λ-shaped anomaly for DTM is observed at $T_N = 0.56$ K, which indicates a phase transition. Below the transition temperature the specific heat curve presents a T^3 behavior (see the inset in Fig. 5), which is characteristic of the contribution of antiferromagnetic magnons in three dimensions [27]. However, due to the restricted temperature range of the fit, we cannot rule out the presence of a more complicated magnetic behavior in this material at low temperatures. For DTF we do not observe any indication of an anomaly in the $C(T)$ curves for temperatures down to 100 mK. Also, no T^{-2} behavior of specific curves is present in these compounds, even for low temperatures, which points out that the nuclear contribution to the specific heat is not relevant at such temperatures.

We estimate the lattice contribution to the specific heat of DTM and DTF from the DTC curve. However, since lattice specific heat is proportional to the mass of the constituents in a lattice site and the compounds have different masses, the DTC curve should be rescaled in order to provide the lattice contribution for the DTM and DTF compounds. Recalling that the Debye temperature is inversely proportional to the square root of the molecular mass, we can introduce a parameter r given by [28]

$$r = \frac{\theta_D^{\mathrm{DTM}}}{\theta_D^{\mathrm{DTC}}} = \sqrt{\frac{M^{\mathrm{DTC}}}{M^{\mathrm{DTM}}}}, \tag{2}$$

which allows us to obtain the lattice contribution to the specific heat of DTM and DTF as

$$C_{\mathrm{latt}}^{\mathrm{DTM(DTF)}}(T) = C_{\mathrm{latt}}^{\mathrm{DTC}}(rT). \tag{3}$$

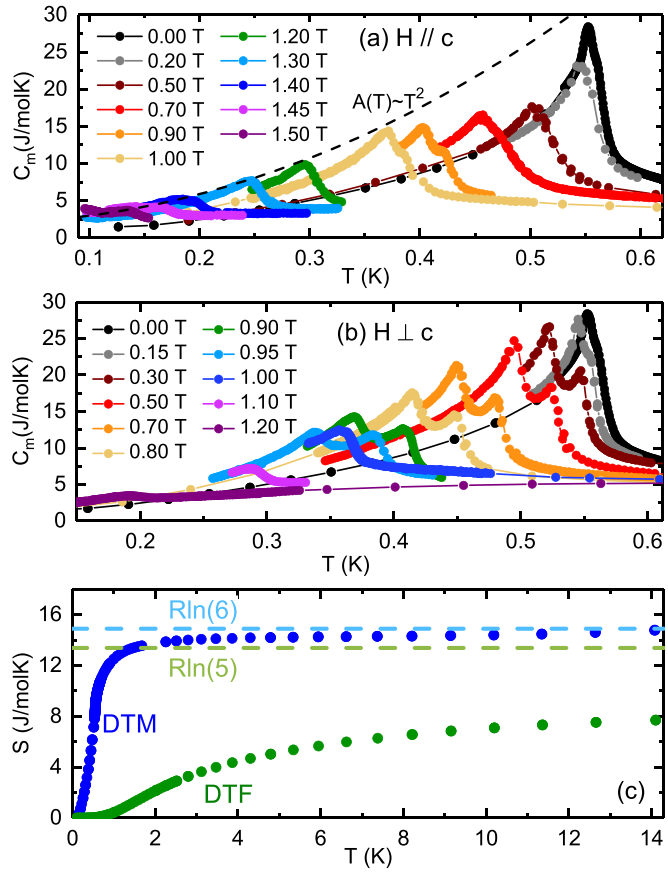

FIG. 6. Magnetic contribution to the specific heat of DTM measured under an applied magnetic field H (a) parallel and (b) perpendicular to the c axis. The dashed line in (a) corresponds to the amplitude $A(T)$ of the specific heat curves according to theoretical predictions (see the text). (c) Magnetic contribution to the entropy obtained by integrating $C_m(T)/T$ for the specific heat curve measured at $\mu_0 H = 0$ T for DTM (blue circles) and DTF (green circles).

By subtracting $C_{\mathrm{latt}}(T)$ from the $C(T)$ curves we obtain the magnetic contribution $C_m(T)$ to the specific heat.

Figure 6 shows the $C_m(T)$ curves for DTM measured at different H for both the $H//c$ and $H \perp c$ orientations.

As commonly observed for antiferromagnets, the presence of an external magnetic field tends to suppress the antiferromagnetic ordering in DTM. Moreover, we observe the existence of two phase transitions in this compound, more clearly for $H \perp c$ measurements. This feature is also present in some examples of antiferromagnetic materials such as the metal dihalide compounds $MnCl_2$ [29,30], NiI_2 [31], $NiCl_2 \cdot 2H_2O$ [32,33], and $NiBr_2 \cdot 2H_2O$ [34]; other similar thiourea ligand compounds like $NiBr_2$-6SC$(NH_2)_2$ [35], NiI_2-6SC$(NH_2)_2$ [36], and the frustrated Ising system $CoCl_2$-2SC$(NH_2)_2$ [37]; and other examples like $K_2PbCu(NO_2)_6$ [38], $Ba_3CoNb_2O_9$ [39], and the thiospinel system $MnSc_2S_4$ [40]. The existence of these successive transitions is frequently related to the presence of non-negligible higher-neighbor interactions and the intricate competition between superexchange mechanisms and anisotropies, which may lead to different magnetic structures [30]. Further experiments, including neutron scattering measurements, are necessary to elucidate the nature of the magnetic orderings in DTM.

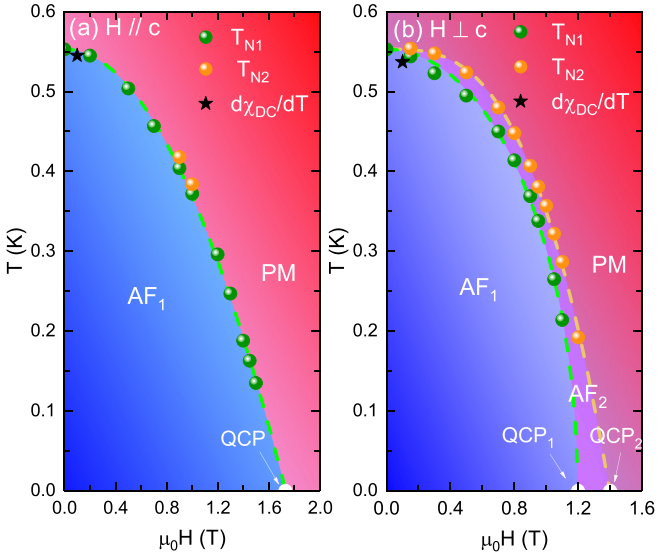

FIG. 7. $H \times T$ phase diagram for DTM obtained from measurements applying the external magnetic field H (a) along the c axis and (b) perpendicular to it, displaying antiferromagnetic phases AF_1 (blue region) and AF_2 (purple region), and the paramagnetic (PM) phase (red region). The phase diagrams were obtained from the peaks of the specific heat curves in Fig. 6 (green and orange points) and from the inflection point of the $\chi_{DC}(T)$ curves in Fig. 4 (black stars).

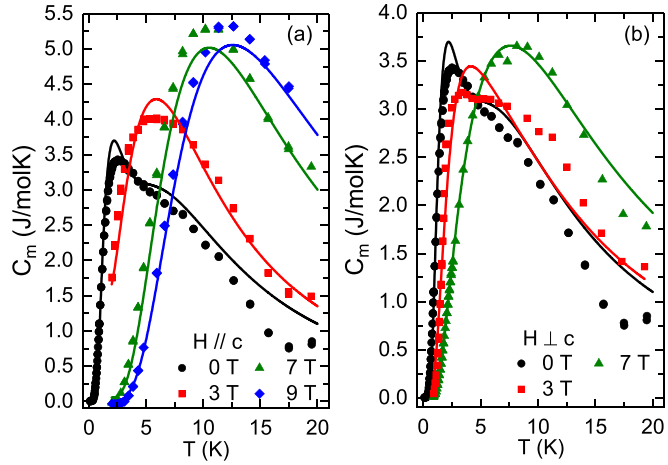

FIG. 8. Magnetic contribution to the specific heat of DTF measured under an applied magnetic field H (a) parallel and (b) perpendicular to the c axis. Solid lines are fits obtained from Eq. (5).

In Fig. 6(c) the curve for the magnetic contribution to the entropy of DTM obtained by integrating $C_m(T)/T$ for $\mu_0 H = 0$ T saturates at $S = R\ln(6)$, which corresponds to the value of entropy of an $S = 5/2$ ideal paramagnetic, and it indicates that the entire magnetic contribution to the entropy was considered in the $C_m(T)$ integration. For DTF we observe a saturation of the entropy curve for a value lower than $S = R\ln(5)$, corresponding to the entropy of an $S = 2$ ideal paramagnet. It indicates that the magnetic ordering of DTF must occur at temperatures even lower than those for our measurements.

From the peaks of $C_m(T)$ curves in Fig. 6 and the inflection points of $\chi_{DC}(T)$ curves in Fig. 4 we present in Fig. 7 the phase diagrams for DTM. The inflection points of $\chi_{DC}(T)$ (black stars) are consistent with the $T_N(H)$ points from the $C_m(T)$ curves, in agreement with the aforementioned theoretical prediction from Ref. [26]. The monotonic dependence of the transition temperatures $T_N(H)$ on the external magnetic field H is fitted as

$$T_N(H) = T_N(0)\left[1 - \left(\frac{H}{H_C}\right)^a\right]^b, \tag{4}$$

where $T_N(0)$ is the Néel temperature at $\mu_0 H = 0$ T and H_C is the critical field at $T = 0$ K.

Remarkably, Eq. (4) provides good fits for the entire phase diagrams in Fig. 7. For a $H//c$ orientation [Fig. 7(a)] a good fit is provided by fixing $b = 1$ and obtaining $a = 1.95(1)$, which is close to the theoretical prediction of $a = 2$, according to mean-field calculations [41] or as obtained from thermodynamic identities [26,42]. In this case, near the critical field H_C, $T_N(H) \propto (H - H_C)^{\psi}$, with a shift exponent $\psi = 1$. Evidence of quantum criticality appears in the decrease of the amplitude of the singular part of the specific heat at the classical transition. Near the critical line $\Delta C(T) \propto T^{2/\psi}|g|^{-\tilde{\alpha}}$, where $g = T - T_N(H)$ and $\tilde{\alpha}$ is the thermal critical exponent of the specific heat [43]. The dashed line in Fig. 6(a) shows a plot of the amplitude $A(T) \propto T^{2/\psi}$ with $\psi = 1$. This gives a reasonable fit of the specific heat amplitude as the quantum critical point is approached.

For the $H \perp c$ orientation [Fig. 7(b)], Eq. (4) fits the points corresponding to T_{N1}, giving $a = 1.95(9)$ and $b = 0.49(2)$. Similar results for exponents a and b were reported for organic magnets in Refs. [44,45] and for the Ising model with antiferromagnetic interactions in different lattices [46]. The best fit of the T_{N2} points is provided by fixing $b = 1$ and obtaining $a = 3.00(5)$.

According to the phase diagram for the $H \perp c$ orientation [Fig. 7(b)] at $T = 0$ K and $\mu_0 H = 0$ T, the system stabilizes in antiferromagnetic phase AF_1. Through the application of an external magnetic field, the system accesses a local energy minimum that corresponds to the phase AF_2, separated from the previous phase by QCP_1. By increasing H the system is driven from phase AF_2 to the paramagnetic phase, separated by QCP_2.

This phase diagram present similarities to the phase diagram for the compound $MnWO_4$, although for this compound the phase diagram presents even more phases due to other relevant interactions and anisotropies of the system. Some theoretical predictions from an $S = 5/2$ anisotropic next-nearest-neighbor Heisenberg model identify the subsequent phases as incommensurate cone and fan antiferromagnetic orderings [47].

While specific heat and magnetization measurements for DTM reveal the existence of a phase transition for this compound, these measurements do not have the same plot for DTF. Figure 8 shows $C_m(T)$ curves at different values of H for the $H//c$ and $H \perp c$ orientations [Figs. 8(a) and 8(b), respectively]. These curves, obtained from $C(T)$ measurements down to $T = 100$ mK, do not present any indication of a phase transition, which would be indicated by the presence of peaks in the $C_m(T)$ curves, but they display broad maxima

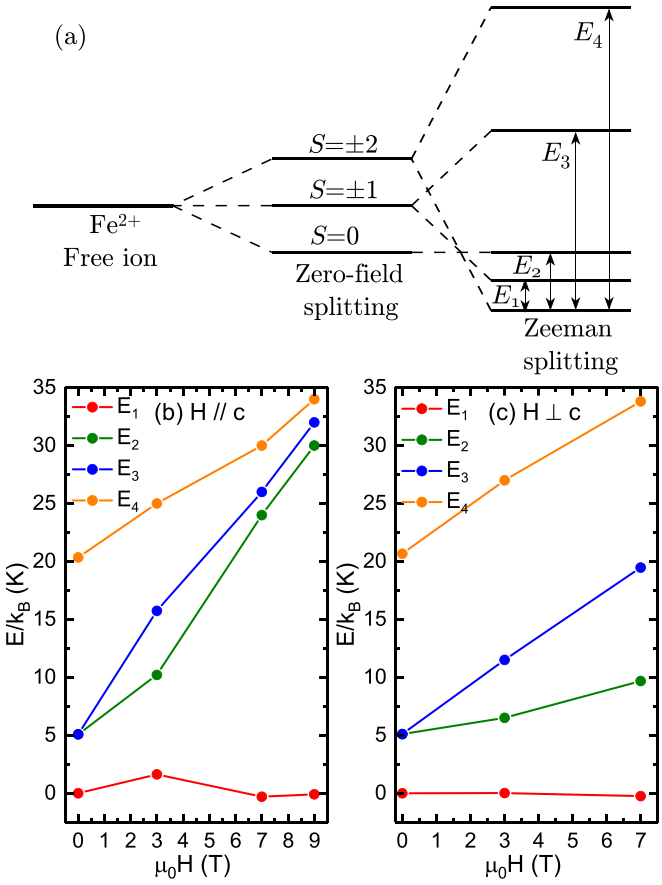

FIG. 9. (a) Schematic representation of the energy levels for a Fe^{2+} ion taking into account the zero-field and Zeeman splittings. Energy levels of DTF obtained from the multilevel Schottky fits to the specific heat curves in Fig. 8 measured for (b) $H//c$ and (c) $H \perp c$.

corresponding to Schottky anomalies. Nevertheless, as estimated from $\chi_{DC}(T)$ in Fig. 2 and summarized in Table I, DTF presents $\theta_{CW} = -10.15$ K in the perpendicular direction, which makes this compound a candidate for a strongly frustrated system with frustration parameter $f = |\theta_{CW}|/T_N > 100$.

The maxima of the $C_m(T)$ curves in Figs. 8(a) and 8(b) are fitted with a multilevel Schottky expression given by [20]

$$C(T) = \frac{N}{k_B T^2}\frac{1}{Z^2}\left[Z\sum_{i=1}^{k} E_i^2 e^{-\beta E_i} - \left(\sum_{i=1}^{k} E_i e^{-\beta E_i}\right)^2\right], \quad (5)$$

where $Z = \sum_{i=1}^{k} e^{-\beta E_i}$ is the partition function and E_i are energy levels depicted in the simplified scheme for the energy levels of an Fe^{2+} ion in Fig. 9(a).

From the fitting of Eq. (5) in the $C_m(T)$ curves in Fig. 8 we obtain the energy levels E_i of the system as a function of H, as presented in Figs. 9(b) and 9(c). The nearly linear aspect of the curves in Figs. 9(b) and 9(c) is consistent with the effect of Zeeman splitting and its linear dependence on the applied magnetic field, which separates the energy levels more the larger the external field is.

We anticipate two possible scenarios to explain the absence of magnetic ordering in DTF. Since the DTF is a spin integer ($S = 2$) system, an energy gap between a nonmagnetic ground state and the lowest-lying exited state is expected according to the Haldane conjecture. The first case we consider is when the gap is open. In this case, the application of external magnetic fields above 9 T can promote the closing of the gap and could lead to a field-induced antiferromagnetic phase, with a QCP possibly from the BEC universality class, like for DTN but for an $S = 2$ compound, which, to the best of our knowledge, has not been observed so far. Additionally, the effects of frustration in DTF and the subsequent degeneracy of the ground state could cause an eventual BEC phase of magnons in this compound to be fragmented in such multiple ground states.

A second possibility for the system concerns the case in which the energy gap is closed. In this situation, due to the strong frustration and the absence of magnetic ordering at low temperatures, DTF is a candidate for a spin-liquid compound. Also, the Fe^{2+} ion in the high-spin $3d^6$ configuration is Jahn-Teller active. For this reason, an orbital ordering in addition to the spin ordering is also a possibility for Fe^{2+}-based systems. However, as we observe for DTF, no indication of magnetic ordering is seen in this compound for temperatures down to 100 mK. For some Fe^{2+}-based systems the possibility of spin-orbital frustration has been discussed [48,49], especially for the compound $FeSc_2S_4$ [40]. So we speculate from the absence of any magnetic ordering from both spin and orbital degrees of freedom that DTF is a candidate for the occurrence of a spin-orbit liquid state. Further studies are needed in order to verify the occurrence of such a state.

IV. CONCLUSIONS

In this work we investigated the metalorganic compounds $MnCl_2$-4SC$(NH_2)_2$ (DTM) and $FeCl_2$-4SC$(NH_2)_2$ (DTF) through magnetic and specific heat measurements. By fitting the experimental results with mean-field theory we got an indication of the antiferromagnetic nature of both compounds.

DTM exhibits a transition to an antiferromagnetic state with $T_N = 0.56$ K. By the application of an external magnetic field H a second transition is observed. In this sense H acts as a tuning parameter for accessing different phases separated by different QCPs. The nature of this second transition is still elusive and demands further studies, especially neutron scattering measurements, to be elucidated.

Despite the value of $\theta_{CW} = -10.15$ K found for DTF, this compound does not show any indication of magnetic ordering for temperatures down to 100 mK, which makes DTF a candidate for a strongly frustrated material with frustration parameter $f > 100$. In the case in which the energy gap is open, we discussed the possibility of a field-induced antiferromagnetic phase, possibly with a BEC QCP, similar to DTN but forming a fragmented BEC of magnons due to the ground state degeneracy of the frustrated system. If the gap is closed, because Fe^{2+}-based compounds are Jahn-Teller active, such an absence of ordering even at low temperatures may suggest the existence of a spin-orbit liquid state in DTF, as also discussed for other Fe^{2+}-based compounds. We hope that our results motivate future studies to explore these possibilities in DTF.

ACKNOWLEDGMENTS

H.F. acknowledges the financial support of Conselho Nacional de Desenvolvimento Científico e Tecnológico (CNPq; Grant No. 141629/2016-9). A.P.-F. acknowledges CNPq (Grant No. 301510/2017-2). M.A.C. acknowledges Fundação de Amparo Pesquisa do Estado do Rio de Janeiro (FAPERJ) and CNPq for partial financial support. R.S.F. acknowledges Fundação de Amparo Pesquisa do Estado de São Paulo (FAPESP; Grant No. 2015/161915) and CNPq (Grant No. 429511/2018-3).

APPENDIX: MAGNETIZATION AND MAGNETIC SUSCEPTIBILITY EXPRESSIONS FOR NONINTERACTING IONS

In this Appendix we present the expressions for the magnetization and magnetic susceptibility of a system of noninteracting ions. We start from the expression of the Hamiltonian of the system, considering only the single-ion anisotropy and the Zeeman term, as

$$\mathcal{H} = D\sum_{\mathbf{r}}\left(S^z_{\mathbf{r}}\right)^2 - g\mu_B H_a \sum_{\mathbf{r}} S^x_{\mathbf{r}} - g\mu_B H_c \sum_{\mathbf{r}} S^z_{\mathbf{r}}, \quad \text{(A1)}$$

where H_a and H_c are the static magnetic fields applied parallel to the a and c axes, respectively.

The calculation of thermodynamic properties is possible by obtaining the eigenenergies of the Hamiltonian. From the eigenenergies E_i we evaluate the partition function, defined as $Z = \sum_i e^{-\beta E_i}$, and obtain the magnetization $M(T,H)$ and the magnetic susceptibility $\chi(T,H)$ as

$$M(T,H) = \frac{1}{\beta}\frac{\partial \ln Z}{\partial H} \quad \text{(A2)}$$

and

$$\chi(T,H) = \frac{\partial M}{\partial H}. \quad \text{(A3)}$$

The calculations considering the magnetic field applied parallel to the c axis are straightforward since in this case the Hamiltonian (A1) is diagonal with eigenvalues given by $E_{m_S} = D(m_S)^2 - g\mu_B H m_S$, where m_S varies from $-S$ to S by an integer value.

However, if we consider the magnetic field applied perpendicular to the c axis the Hamiltonian is not diagonal, and some analytical or numerical efforts are necessary to obtain its eigenenergies. In this case, we obtain the $M(T,H)$ expressions by numerically diagonalizing the Hamiltonian in (A1) and calculating the magnetization according to (A2).

In the following we present the expressions for the magnetization $M_c(T,H)$ with the magnetic field applied parallel to the c axis as well as the expressions for parallel χ_c and perpendicular χ_a zero-field magnetic susceptibilities for $S = 1$, $S = 2$, and $S = 5/2$ systems.

For a spin-1 system the magnetization, according to (A2) is given by

$$M_c(T,H) = Ng\mu_B\left[\frac{2\exp(-D\beta)\sinh(\beta g_z\mu_B H)}{1+2\exp(-D\beta)\cosh(\beta g_z\mu_B H)}\right]. \quad \text{(A4)}$$

The zero-field magnetic susceptibilities, from Eq. (A3), are

$$\chi_c(T,H=0) = \frac{2Ng^2\mu_B^2}{k_BT}\left[\frac{\exp(-D\beta)}{1+2\exp(-D\beta)}\right] \quad \text{(A5)}$$

and

$$\chi_a(T,H=0) = \frac{2Ng^2\mu_B^2}{D}\left[\frac{1-\exp(-D\beta)}{1+2\exp(-D\beta)}\right]. \quad \text{(A6)}$$

For a spin-2 system we have

$$M_c(T,H) = Ng_z\mu_B\left[\frac{4\exp(-4D\beta)\sinh(2\beta g_z\mu_B H)+2\exp(-D\beta)\sinh(\beta g_z\mu_B H)}{2\exp(-4D\beta)\cosh(2\beta g_z\mu_B H)+2\exp(-D\beta)\cosh(\beta g_z\mu_B H)+1}\right], \quad \text{(A7)}$$

$$\chi_c(T,H=0) = \frac{Ng^2\mu_B^2}{k_BT}\left[\frac{2\exp(-D\beta)+8\exp(-4D\beta)}{1+2\exp(-2D\beta)+2\exp(-4D\beta)}\right], \quad \text{(A8)}$$

and [50–52]

$$\chi_a(T,H=0) = \frac{Ng^2\mu_B^2}{k_BT}\left[\frac{\frac{6k_BT}{D}[1-\exp(-D\beta)]+\frac{4D}{3k_BT}[\exp(-D\beta)-\exp(-4D\beta)]}{1+2\exp(-2D\beta)+2\exp(-4D\beta)}\right]. \quad \text{(A9)}$$

Finally, we have, for a spin-5/2 system, the following expressions:

$$M_c(T,H) = \frac{Ng_z\mu_B}{2}\left[\frac{5\exp(-6D\beta)\sinh\left(\frac{5}{2}\beta g_z\mu_B H\right)+3\exp(-2D\beta)\sinh\left(\frac{3}{2}\beta g_z\mu_B H\right)+\sinh\left(\frac{1}{2}\beta g_z\mu_B H\right)}{\exp(-6D\beta)\cosh\left(\frac{5}{2}\beta g_z\mu_B H\right)+\exp(-2D\beta)\cosh\left(\frac{3}{2}\beta g_z\mu_B H\right)+\cosh\left(\frac{1}{2}\beta g_z\mu_B H\right)}\right], \quad \text{(A10)}$$

$$\chi_c(T,H=0) = \frac{Ng^2\mu_B^2}{4k_BT}\left[\frac{1+9\exp(-2D\beta)+25\exp(-6D\beta)}{1+\exp(-2D\beta)+\exp(-6D\beta)}\right], \quad \text{(A11)}$$

and [24,51,52]

$$\chi_a(T,H=0) = \frac{Ng^2\mu_B^2}{4k_BT}\left[\frac{\left(\frac{9}{k_BT}+\frac{8}{D}\right)-\frac{11}{2D}\exp(-2D\beta)-\frac{5}{2D}\exp(-6D\beta)}{1+\exp(-2D\beta)+\exp(-6D\beta)}\right]. \quad \text{(A12)}$$

[1] M. H. Anderson, J. R. Ensher, M. R. Matthews, C. H. Weiman, and E. A. Cornell, Science **269**, 198 (1995).

[2] K. B. Davis, M. O. Mewes, M. R. Andrews, N. J. van Druten, D. S. Durfee, D. M. Kurn, and W. Ketterle, Phys. Rev. Lett. **75**, 3969 (1995).

[3] J. Kasprzak, M. Richard, S. Kundermann, A. Baas, P. Jeambrun, J. M. J. Keeling, F. M. Marchetti, M. H. Szymańska, R. André, J. L. Staehli, V. Savona, P. B. Littlewood, B. Deveaud, and L. S. Dang, Nature (London) **443**, 409 (2006).

[4] S. O. Demokritov, V. E. Demidov, O. Dzyapko, G. A. Melkov, A. A. Serga, B. Hillebrands, and A. N. Slavin, Nature (London) **443**, 430 (2006).

[5] V. Zapf, M. Jaime, and C. D. Batista, Rev. Mod. Phys. **86**, 563 (2014).

[6] A. Paduan-Filho, X. Gratens, and N. F. Oliveira, Jr., Phys. Rev. B **69**, 020405(R) (2004).

[7] V. S. Zapf, D. Zocco, B. R. Hansen, M. Jaime, N. Harrison, C. D. Batista, M. Kenzelmann, C. Niedermayer, A. Lacerda, and A. Paduan-Filho, Phys. Rev. Lett. **96**, 077204 (2006).

[8] S. A. Zvyagin, J. Wosnitza, C. D. Batista, M. Tsukamoto, N. Kawashima, J. Krzystek, V. S. Zapf, M. Jaime, N. F. Oliveira, Jr., and A. Paduan-Filho, Phys. Rev. Lett. **98**, 047205 (2007).

[9] R. Yu, L. Yin, N. S. Sullivan, J. S. Xia, C. Huan, A. Paduan-Filho, N. F. Oliveira Jr., S. Haas, A. Steppke, C. F. Miclea, F. Weickert, R. Movshovich, E.-D. Mun, B. L. Scott, V. S. Zapf, and T. Roscilde, Nature (London) **489**, 379 (2012).

[10] A. Oosawa, M. Fujisawa, T. Osakabe, K. Kakurai, and H. Tanaka, J. Phys. Soc. Jpn. **72**, 1026 (2003).

[11] A. Oosawa, K. Kakurai, T. Osakabe, M. Nakamura, M. Takeda, and H. Tanaka, J. Phys. Soc. Jpn. **73**, 1446 (2004).

[12] K. Goto, M. Fujisawa, T. Ono, H. Tanaka, and Y. Uwatoko, J. Phys. Soc. Jpn. **73**, 3254 (2004).

[13] Ch. Rüegg, A. Furrer, D. Sheptyakov, Th. Strässle, K. W. Krämer, H.-U. Güdel, and L. Mélési, Phys. Rev. Lett. **93**, 257201 (2004).

[14] Ch. Rüegg, B. Normand, M. Matsumoto, A. Furrer, D. F. McMorrow, K. W. Krämer, H.-U. Güdel, S. N. Gvasaliya, H. Mutka, and M. Boehm, Phys. Rev. Lett. **100**, 205701 (2008).

[15] T. Hong, V. O. Garlea, A. Zheludev, J. A. Fernandez-Baca, H. Manaka, S. Chang, J. B. Leao, and S. J. Poulton, Phys. Rev. B **78**, 224409 (2008).

[16] T. Hong, C. Stock, I. Cabrera, C. Broholm, Y. Qiu, J. B. Leao, S. J. Poulton, and J. R. D. Copley, Phys. Rev. B **82**, 184424 (2010).

[17] N. Kurita and H. Tanaka, Phys. Rev. B **94**, 104409 (2016).

[18] S. E. Sebastian, N. Harrison, C. D. Batista, L. Balicas, M. Jaime, P. A. Sharma, N. Kawashima, and I. R. Fisher, Nature (London) **441**, 617 (2006).

[19] H. J. Van Till, Ph.D. thesis, Michigan State University, 1965.

[20] J. Shi, H. S. Xu, L. M. Chen, J. D. Song, J. C. Wu, X. G. Liu, X. Zhao, and X. F. Sun, J. Cryst. Growth **451**, 6 (2016).

[21] M. Gerloch, J. Lewis, and W. R. Smail, J. Chem. Soc., Dalton Trans. **14**, 1559 (1972).

[22] U. Russo, R. Graziani, S. Calogero, and U. Casellato, Transition Met. Chem. (Dordrecht, Neth.) **4**, 82 (1979).

[23] P. J. McCarthy and I. M. Walker, Can. J. Chem. **56**, 1284 (1978).

[24] O. Kahn, *Molecular Magnetism* (Wiley-VHC, New York, 1993).

[25] C. Kittel, *Introduction to Solid State Physics*, 8th ed. (Wiley, New York, 2005).

[26] M. A. Fisher, Philos. Mag. **7**, 1731 (1962).

[27] A. Tari, *The Specific Heat of Matter at Low Temperatures* (Imperial College Press, London, 2003).

[28] V. Hardy, S. Lambert, M. R. Lees, and D. McK. Paul, Phys. Rev. B **68**, 014424 (2003).

[29] R. B. Murray, Phys. Rev. **100**, 1071 (1955).

[30] D. G. Wiesler, M. Suzuki, I. S. Suzuki, and N. Rosov, Phys. Rev. Lett. **75**, 942 (1995).

[31] D. Billerey, C. Terrier, N. Ciret, and J. Kleinclauss, Phys. Lett. A **61**, 138 (1977).

[32] L. G. Polgar, A. Herweijer, and W. J. M. de Jonge, Phys. Rev. B **5**, 1957 (1972).

[33] C. H. W. Swüste, A. C. Botterman, J. Millenaar, and W. J. M. de Jonge, J. Chem. Phys. **66**, 5021 (1977).

[34] K. Kopinga and W. J. M. de Jonge, Phys. Lett. A **43**, 415 (1973).

[35] H. Forstat, N. D. Love, and J. McElearney, J. Chem. Phys. **43**, 1626 (1965).

[36] H. Forstat, N. D. Love, and J. McElearney, J. Phys. Soc. Jpn. **23**, 229 (1967).

[37] E. Mun, F. Weickert, J. Kim, B. L. Scott, C. F. Miclea, R. Movshovich, J. Wilcox, J. Manson, and V. S. Zapf, Phys. Rev. B **93**, 104407 (2016).

[38] N. Blanc, J. Trinh, L. Dong, X. Bai, A. A. Aczel, M. Mourigal, L. Balents, T. Siegrist, and A. P. Ramirez, Nat. Phys. **14**, 273 (2018).

[39] K. Yokota, N. Kurita, and H. Tanaka, Phys. Rev. B **90**, 014403 (2014).

[40] V. Fritsch, J. Hemberger, N. Büttgen, E.-W. Scheidt, H.-A. Krug von Nidda, A. Loidl, and V. Tsurkan, Phys. Rev. Lett. **92**, 116401 (2004).

[41] Y. Shapira and S. Foner, Phys. Rev. B **1**, 3083 (1970).

[42] J. Skalyo, A. F. Cohen, S. A. Friedberg, and R. B. Griffiths, Phys. Rev. **164**, 705 (1967).

[43] P. Chandra, P. Coleman, M. A. Continentino, and G. G. Lonzarich, Phys. Rev. Research **2**, 043440 (2020).

[44] K. Takeda, Y. Yoshida, Y. Inanaga, T. Kawae, D. Shiomi, T. Ise, M. Kozaki, K. Okada, K. Sato, and T. Takui, Phys. Rev. B **72**, 024435 (2005).

[45] H. Murata, Y. Miyazaki, A. Inaba, A. Paduan-Filho, V. Bindilatti, N. F. Oliveira, Z. Delen, and P. M. Lahti, J. Am. Chem. Soc. **130**, 186 (2008).

[46] A. Bienenstock, J. Appl. Phys. **37**, 1459 (1966).

[47] M. V. Gvozdikova, T. Ziman, and M. E. Zhitomirsky, Phys. Rev. B **94**, 020406(R) (2016).

[48] G. Perversi, A. M. Arevalo-Lopez, C. Ritter, and J. P. Attfield, Commun. Phys. **1**, 69 (2018).

[49] F. Krüger, S. Kumar, J. Zaanen, and J. van den Brink, Phys. Rev. B **79**, 054504 (2009).

[50] X.-Y. Xing, X.-L. Mei, and L.-C. Li, J. Mol. Struct. **992**, 89 (2011).

[51] R. Boča, Coord. Chem. Rev. **248**, 757 (2004).

[52] R. Pełka, Acta Phys. Pol. A **119**, 428 (2011).